Climatic Change (2008) 89:45–66
DOI 10.1007/s10584-008-9421-1

Learning about the ocean carbon cycle from observational constraints and model simulations of multiple tracers

Long Cao · Atul K. Jain

Received: 29 January 2007 / Accepted: 19 March 2008 / Published online: 29 April 2008

Abstract A key question in studies of the potential for reducing uncertainty in climate change projections is how additional observations may be used to constrain models. We examine the case of ocean carbon cycle models. The reliability of ocean models in projecting oceanic CO_2 uptake is fundamentally dependent on their skills in simulating ocean circulation and air–sea gas exchange. In this study we demonstrate how a model simulation of multiple tracers and utilization of a variety of observational data help us to obtain additional information about the parameterization of ocean circulation and air–sea gas exchange, relative to approaches that use only a single tracer. The benefit of using multiple tracers is based on the fact that individual tracer holds unique information with regard to ocean mixing, circulation, and air–sea gas exchange. In a previous modeling study, we have shown that the simulation of radiocarbon enables us to identify the importance of parameterizing sub-grid scale ocean mixing processes in terms of diffusive mixing along constant density surface (isopycnal mixing) and the inclusion of the effect of mesoscale eddies. In this study we show that the simulation of phosphate, a major macronutrient in the ocean, helps us to detect a weak isopycnal mixing in the upper ocean that does not show up in the radiocarbon simulation. We also show that the simulation of chlorofluorocarbons (CFCs) reveals excessive upwelling in the Southern Ocean, which is also not apparent in radiocarbon simulations. Furthermore, the updated ocean inventory data of man-made radiocarbon produced by nuclear tests (bomb ^{14}C) enable us to recalibrate the rate of air–sea gas exchange. The progressive modifications made in the model based on the simulation of additional tracers and utilization of updated observational data overall improve the model's ability to simulate ocean circulation and air–sea gas exchange, particularly in the Southern Ocean, and has great consequence for projected CO_2 uptake. Simulated global ocean uptake of anthropogenic CO_2 from pre-industrial time to

L. Cao · A. K. Jain (✉)
Department of Atmospheric Sciences, University of Illinois, Urbana, IL, USA
e-mail: jain@atmos.uiuc.edu

Present address:
L. Cao
Department of Global Ecology, Carnegie Institution, Stanford, CA, USA

the present day by both previous and updated models are within the range of observational-based estimates, but with substantial regional difference, especially in the Southern Ocean. By year 2100, the updated model estimated CO_2 uptake are 531 and 133 PgC (1PgC=10^{15} gram carbon) for the global and Southern Ocean respectively, whereas the previous version model estimated values are 540 and 190 PgC.

1 Introduction

An accurate projection of atmospheric CO_2 concentrations is a prerequisite to reliably project future climate change. The rate of increase in atmospheric CO_2 depends on CO_2 emissions due to human activities and the rate of the ocean and terrestrial biosphere to take up emitted CO_2 (Prentice et al. 2001). The ocean plays a fundamental role in regulating atmospheric CO_2 concentrations on a variety of timescales ranging from seasons to tens of thousands of years. Over the past two and a half centuries the ocean has absorbed about one third of the anthropogenic CO_2 emissions produced from fossil fuel burning, cement production, and land-use change (Sabine et al. 2004), and it will continue to serve as a major sink reservoir for anthropogenic carbon within the coming centuries (Kheshgi and Jain 2003).

Numerical models have become essential tools to characterize the behavior of the ocean carbon cycle and its response to increasing atmospheric CO_2 concentrations. Since their early emergence in the 1970s, a hierarchy of ocean carbon cycle models has been developed, ranging from globally averaged 1-D models (e.g., Oeschger et al. 1975; Siegenthaler and Joos 1992; Jain et al. 1995; Harvey 2001) and zonally averaged ocean models (e.g., Stocker et al. 1994; Marchal et al. 1998; Joos et al. 1999; Cao and Jain 2005) to 3-D general ocean circulation models (OGCMs) (e.g., Sarmiento et al. 1992; Maier-Reimer 1993; Orr et al. 2001; Müller et al. 2006). As pointed out by two recent studies (Matsumoto et al. 2004; Doney et al. 2004) assessing the performance of a suite of ocean carbon models, many ocean models used to project oceanic uptake of anthropogenic CO_2 fall noticeably outside observational constraints when evaluated against observational-based metrics such as temperature, salinity, radiocarbon, and chlorofluorocarbons (CFCs). This challenges the reliability of projections by these models of the amount of anthropogenic CO_2 absorbed by the ocean..

The purpose of this study is to investigate how the representation of ocean mixing and air–sea gas exchange can be improved through the simulation of multiple tracers and the inclusion of updated observational constraints. Gas exchange and ocean mixing, along with carbon chemistry and biological activity, are the key factors governing carbon uptake by the ocean. In general, previous studies have made use of different chemical tracers to assess and constrain parameterizations of ocean mixing and air–sea gas exchange (see a review of England and Maier-Reimer 2001). Many modeling studies simulated a single tracer such as radiocarbon (e.g. Toggweiler et al. 1989a, 1989b; Duffy et al. 1997; England and Rahmstorf 1999; Guilderson et al. 2000) and CFCs (e.g., Robitaille and Weaver 1995; Dutay et al. 2002). A few studies simulated multiple tracers (e.g. Maier-Reimer 1993; Orr et al. 2001; Müller et al. 2006), but the question remains whether and how the simulation of multiple tracers can provide complementary information about model parameterizations of ocean mixing and air–sea gas exchange.

In this study we aim to address the above question by simulating a variety of tracers including natural radiocarbon (^{14}C produced naturally by cosmic rays in the upper atmosphere), phosphate (a major nutrient in the ocean that sustains biological productivity

and affects the distribution of carbon in the ocean), bomb radiocarbon (man-made ^{14}C produced by nuclear tests during early 1960s), anthropogenic CO_2, and chlorofluorocarbons (CFC11 here) using an earth system model of intermediate complexity (Cao and Jain 2005). Different tracers are affected differently by ocean circulation and air–sea gas exchange and therefore they can provide complementary information about these two processes. For example, as discussed in detail in section 3.1, because radiocarbon (in terms of $\Delta^{14}C$ that is primarily related to the ratio of $^{14}C/^{12}C$, see Appendix A) and phosphate have different sensitivities to biological processes, they hold different information about ocean mixing and circulation through feedbacks between ocean dynamics and biology. Similarly, because anthropogenic (or "transient") tracers (bomb radiocarbon, anthropogenic CO_2, and chlorofluorocarbons) have different timescales of air–sea equilibration and their atmospheric concentrations have evolved differently over time, the simulation of these tracers test different aspects of modeled air–sea gas exchange and ocean circulation. This work is built upon our previous study (Cao and Jain 2005) in which we have constrained an ocean carbon cycle model by simulating natural radiocarbon, bomb radiocarbon, and CO_2. In this study we first examine the role of simulating phosphate in further constraining model parameterization of ocean mixing that has been tested by the simulation of radiocarbon. We then investigate what new information can be obtained about the rate of air–sea exchange and/or ocean mixing based on updated estimates of oceanic uptake for transient tracers (Key et al. 2004). Furthermore, we explore additional information about model parameterization of ocean circulation and air–sea exchange through the simulation of CFC11, in addition to bomb ^{14}C and anthropogenic CO_2.

Our study illustrates a learning process in which new information is brought to bear on the representation of ocean circulation and air–sea gas exchange in ocean carbon cycle models, leading to changes in model structure and simulated carbon uptake. Melnikov and O'Neill (2006) and O'Neill and Melnikov (2007, in this volume) examine how learning about the structure and parameter values of a globally aggregated carbon cycle could take place via updated observations of carbon emissions and atmospheric concentrations over time. Here, we investigate how additional information in the form of multiple tracers can be used to foster the learning about carbon cycle modeling using an earth system model of intermediate complexity.

The paper is organized as follows. In section 2, we briefly describe the model used in this study. In section 3, we discuss new insights gained about representations of ocean circulation and air–sea gas exchange in the model after the inclusion of additional tracers and updated observations, as well as the implications for carbon uptake. Discussion and conclusions follow in section 4.

2 Model description

In this study we use an earth system model of intermediate complexity, the Integrated Science Assessment Model (ISAM-2.5D) (Cao and Jain 2005). The ISAM-2.5D is represented by a zonally averaged multi-basin dynamic ocean component that couples to an organic and inorganic carbon cycle model with explicit representation of marine biology, in addition to an atmosphere and sea ice components. Despite the reduced resolution of ocean geography and simplified representation of atmosphere and ocean dynamics in the model relative to comprehensive 3-D models, the model captures key processes relevant to ocean dynamics and carbon uptake including different mixing processes (as detailed in section 3.1) and air–sea gas exchange. Therefore, insights gained from this study will have broad

implications for ocean carbon cycle modeling communities, including comprehensive 3-D modeling studies.

3 Learning about ocean circulation and air–sea gas exchange

In this section we discuss insights gained about the ocean component of the ISAM-2.5D model and modifications made in model parameterizations after the simulations of multiple tracers and inclusion of updated observational data. We first identify problems in the parameterization of ocean diffusive mixing based on the simulation of phosphate. We then update the parameterization of air–sea gas exchange using updated bomb ^{14}C data. Finally, we suggest modification in the parameterization of mesoscale eddies through the simulation of CFC11. Table 1 summarizes various model simulations and Table 2 lists model parameters used in each simulation as a result of updated model calibration after the addition of new tracers and observations.

3.1 Simulate phosphate

Subgrid-scale mixing processes and mesoscale eddies cannot be explicitly accounted for in coarse resolution ocean circulation models and thus mixing parameterization schemes are required to represent these processes. The simulation of radiocarbon (^{14}C) is often used to assess the performance of different mixing schemes in ocean circulation models (e.g., Duffy et al. 1997; England and Rahmstorf 1999; Cao and Jain 2005). Through the simulation of $\Delta^{14}C$ (ISAM run), Cao and Jain (2005) concluded that to achieve a realistic simulation of $\Delta^{14}C$ distribution, especially in the Southern Ocean, ocean subgrid-scale processes should be parameterized using both diffusive mixing along constant density surfaces (also known as isopycnal diffusion, see Redi 1982) and including mixing due to mesoscale eddies (Gent et al. 1995; Gent-McWilliams (GM) scheme) that parameterizes the effect of mesoscale eddies on large-scale circulation in terms of large-scale density. Two key parameters involved in these parameterization schemes are isopycnal diffusivity (K_I), which determines the strength of isopycnal diffusion, and isopycnal thickness diffusivity (GM parameter, K_{GM}), which determines the strength of eddy-induced circulation. Data-based determination of these two parameters requires direct observation of tracer distributions and circulation fields on the spatial scale of mesoscale eddies, which is not currently feasible at the global scale. As a first order approximation, Cao and Jain (2005) use a globally uniform value of 1.0×10^3 m^2 s^{-1} for both parameters (Gent et al. 1995).

Here we aim to test whether the simulation of biogeochemical tracers, such as phosphate, can provide more information about the parameterization of ocean mixing. The motivation behind this test is that phosphate and $\Delta^{14}C$ hold different information about ocean circulation as a result of their different sensitivities to biological processes and intrinsic links between marine biology and ocean circulation. $\Delta^{14}C$, being primarily related to the ratio of ^{14}C to ^{12}C, is only affected by ocean mixing and insensitive to biological processes because they affect ^{14}C and ^{12}C in the same manner (Fiadeiro 1982). In contrast, phosphate, being one of the major nutrients to sustain biological productivity in the ocean, is affected not only by ocean mixing, but also by biological processes such as the conversion between organic and inorganic matter through photosynthesis and decomposition. These biological processes are strongly mediated by ocean mixing and circulation; e.g., upwelling brings nutrients to ocean surface to fuel biological production, while horizontal mixing and transport carry away the nutrients from where they are produced.

Table 1 Tabulate description of the learning process about the representation of ocean mixing and air-sea exchange in ISAM model

Tracer simulated and/or new observation used	Parameterizations of ocean mixing and air–sea exchange identified that needs to be included and/or modified	Name of model runs	Key model features relevant to the representation of ocean mixing and air–sea gas exchange
Simulate $\Delta^{14}C$	Isopycnal diffusion and eddy-induced circulation	ISAM (1)	The model of Cao and Jain (2005) with constant isopycnal diffusivity and GM parameter. The rate of air–sea exchange is calibrated based on the bomb ^{14}C inventory data of Broecker et al (1985, 1995).
Simulate phosphate	Isopycnal diffusivity	ISAM+OCMIP (2a) ISAM+DGOM (2b) ISAM+OCMIP+updateK_I (3a) ISAM-DGOM+updateK_I (3b)	Same as (1), but with the inclusion of OCMIP or DGOM biological component. Same as 2a(2b), but with depth-dependent isopycnal diffusivity.
Use updated bomb ^{14}C inventory	The rate of air–sea exchange	ISAM+OCMIP +updateK_I+updateKgas (4)	Same as (3a), but with the rate of air–sea gas exchange calibrated based on the updated bomb C inventory data of Key et al (2004).
Simulate CFC11	GM parameter used in the parameterization of eddy-induced circulation	ISAM+OCMIP +updateK_I+updateKgas+ updateK_{GM} (5)	Same as (4), but the GM parameter is calculated as a function of density based on Visbeck et al. (1997) and Marshall and Radko (2003).

Table 2 Parameters of ocean mixing and air–sea gas exchange used in different runs of the ISAM-2.5D model as listed in Table 1

Model runs	Isopycnal diffusivity ($m^2\ s^{-1}$) (K_I)	GM parameter (K_{GM}) ($m^2\ s^{-1}$)	Scaling factor (f) in the rate of air–sea gas exchange (K_{gas})			
			Atlantic	Pacific	Indian	Southern
ISAM	1.0×10^3	1.0×10^3	0.50	0.50	0.50	0.50
ISAM+OCMIP	1.0×10^3	1.0×10^3	0.50	0.50	0.50	0.50
ISAM+DGOM						
ISAM+OCMIP+updateK$_I$	7.0×10^3 to 1.0×10^3 $m^2\ s^1$	1.0×10^3	0.50	0.50	0.50	0.50
ISAM+DGOM+updateK$_I$	from ocean surface to bottom					
ISAM+OCMIP +updateK$_I$+updateKgas	7.0×10^3 to 1.0×10^3 $m^2\ s^1$ from ocean surface to bottom	1.0×10^3	0.50	0.54	0.58	0.23
ISAM+OCMIP +updateK$_I$+updateKgas+updateK$_{GM}$	7.0×10^3 to 1.0×10^3 $m^2\ s^1$ from ocean surface to bottom	between 0.8 and 2.0×10^3	0.50	0.54	0.58	0.23

Therefore ocean dynamics, through its effect on biological processes, affects the distribution of biological tracers more than the distribution of $\Delta^{14}C$. In other words, weaknesses in modeled ocean circulation and mixing not readily visible in the simulation of $\Delta^{14}C$ might be exposed more clearly through the simulation of biological tracers like phosphate.

To explore the role of simulating phosphate in further constraining $\Delta^{14}C$-calibrated parameterization of ocean mixing, we conducted two runs including the simulation of marine biology using the ISAM-2.5D model calibrated by the simulation of $\Delta^{14}C$. The purpose of these simulations is to investigate whether the simulation of phosphate can identify problems in the parameterization of ocean mixing that is not detected by the simulation of $\Delta^{14}C$. To test the sensitivity of our results to the representation of biogeochemical processes, we have incorporated two distinct biogeochemical models into the ISAM-2.5D: a geochemical model based on the Ocean Carbon-Cycle Model Intercomparison Project (OCMIP) protocol that simply parameterizes biological processes in terms of geochemical fluxes (http://www.ipsl.jussieu.fr/OCMIP) (referred to as OCMIP model hereafter); and a marine ecosystem model based on Le Quéré et al. (2005) that explicitly represents a suite of biological and food web processes (referred to as the Dynamic Green Ocean Model (DGOM) hereafter). Details on both models are given in Appendix B. The simulations with these two model are listed here as ISAM+OCMIP and ISAM+DGOM.

The ISAM+OCMIP model-simulated latitude-depth distribution of phosphate concentrations show more pronounced model-observation discrepancy than that of $\Delta^{14}C$ (Fig. 1). In particular, in the upper 200 m ocean around 10°S the ISAM+OCMIP run overestimates the phosphate concentration by a factor of more than two, while the simulated $\Delta^{14}C$ is greater than the observation by less than 20%. Likewise, the ISAM+DGOM run overestimates the phosphate concentration in the uppermost 100 m low latitude ocean by a factor of nearly three while the modeled $\Delta^{14}C$ in that region is comparable to the observation (Fig. 2). The excess accumulation of phosphate in both model runs can be explained as follows: the accumulation of phosphate concentrations in the upper low latitude ocean initialized by dynamic processes (e.g., overly strong upwelling of phosphate-rich deep ocean waters and/or insufficient horizontal mixing with surrounding phosphate-poor waters) leads to intense biological production and excess organic matter. The organic matter is subsequently decomposed into inorganic nutrients including phosphate and carbon at ocean depth, which is then brought back to the upper ocean through upwelling and mixing. The excess buildup of phosphate concentrations, similar to the "nutrient trapping" problem found in previous studies (e.g., Najjar et al. 1992; Anderson and Sarmiento 1995; Aumont et al. 1999), is therefore a consequence of the interaction between ocean dynamics and biological processes. Since this interaction does not affect $\Delta^{14}C$, this problem does not show up in $\Delta^{14}C$ distribution.

Previous studies argued that the problem of "nutrient trapping" is a result of the lack of dissolved organic matter (DOM) in ocean models (e.g., Bacastow and Maier-Reimer 1990; Najjar et al. 1992; Anderson and Sarmiento 1995). Aumont et al. (1999), in contrast, found that deficiencies in modeled circulation fields are mainly responsible for the "nutrient trapping" problem. DOM has been included in both ISAM+OCMIP and ISAM+DGOM runs and thus the excessive buildup of phosphate is not a result of the lack of DOM in our model simulations. Extensive sensitivity experiments in the ISAM+OCMIP and ISAM + DGOM runs involving modifications in biological parameters (e.g., the rate of growth and remineralization of organic matter, the lifetime and decomposition depth of DOM, and parameters related to plankton dynamics) show that changes in biological parameters cannot

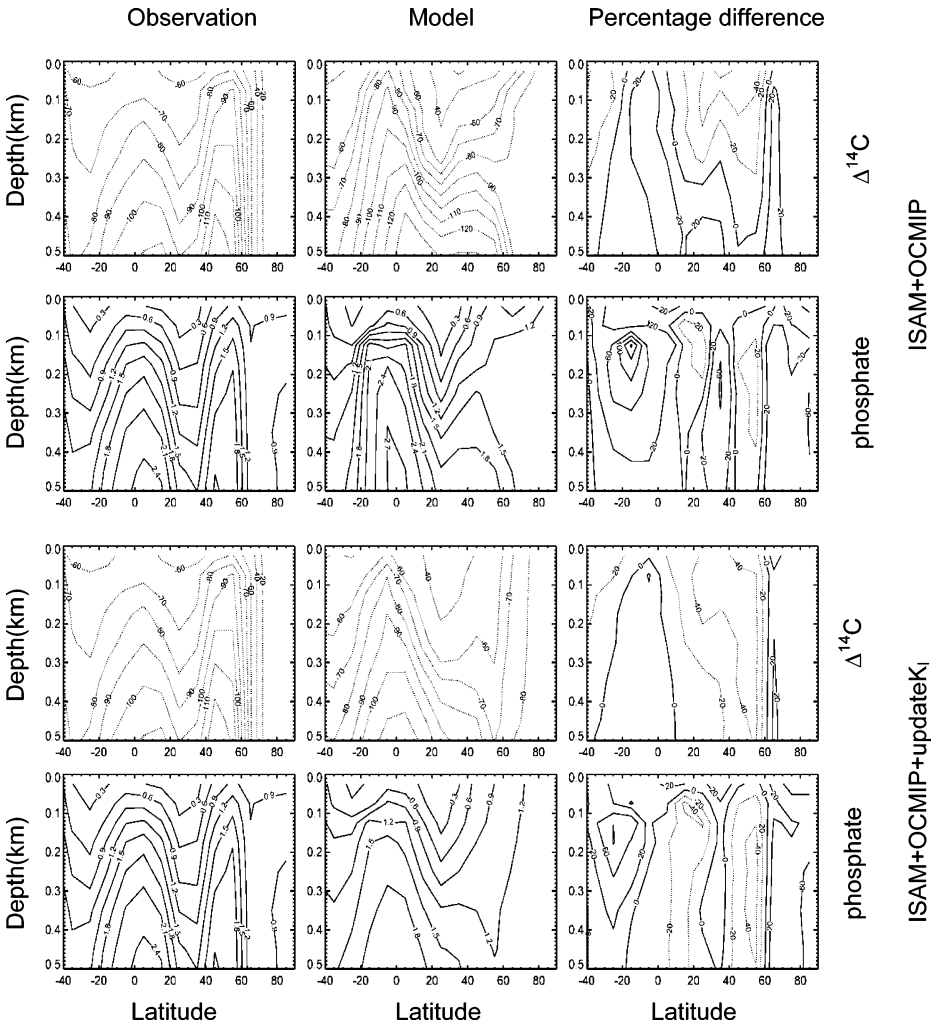

Fig. 1 Latitude-depth distribution of $\Delta^{14}C$ (per mil) and phosphate (micromole per kilogram) over the uppermost 500 m of the global ocean for the observation ($\Delta^{14}C$ from Key et al. 2004 and phosphate from Conkright et al. 2002), model simulations of ISAM+OCMIP and ISAM+OCMIP+updateK_I runs, and the percentage difference between model simulations and corresponding observations

improve the phosphate distribution in the low latitude region without severely worsening its distribution in mid-to-high latitude oceans, indicating that problems in the model parameterizations of ocean mixing is responsible for the excessive accumulation of phosphate concentrations. We identified that weak isopycnal diffusion at the upper ocean is mainly responsible for the excess accumulation of phosphate in the low latitude region. To improve phosphate simulation, we enhance isopycnal diffusivity in the upper ocean by replacing the uniform isopycnal diffusivity of 1.0×10^3 m^2 s^{-1} used in the ISAM+OCMIP and ISAM+DGOM model with a depth-dependent profile that decreases with depth. Sensitivity studies show that an isopycnal diffusivity decreasing exponentially from 7.0×10^3 m^2 s^{-1} at the surface ocean to 1.0×10^3 m^2 s^{-1} at bottom ocean yields an improved simulation of phosphate

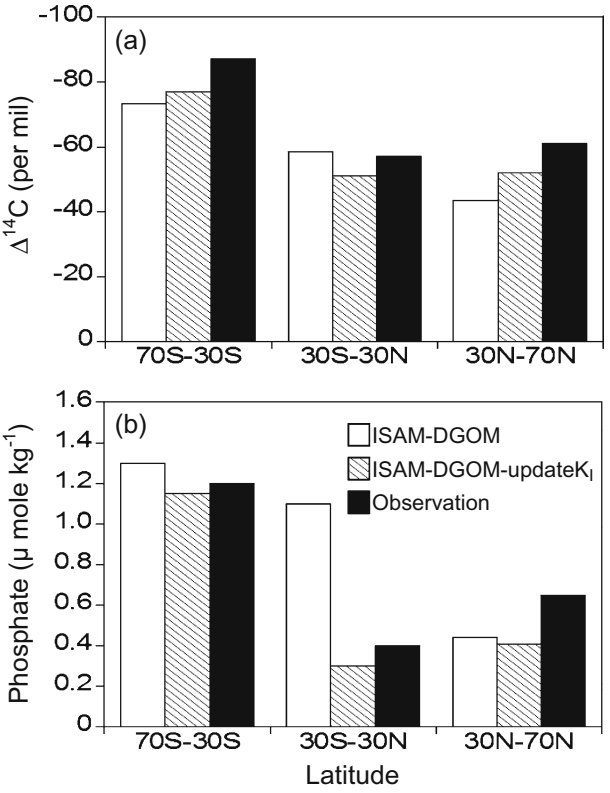

Fig. 2 Averaged (**a**) $\Delta^{14}C$ (per mil) and (**b**) phosphate concentrations over the uppermost 100 m of the ocean simulated by the ISAM+DGOM and ISAM+DGOM+updateK_I runs. Corresponding data-based estimates of $\Delta^{14}C$ (Key et al. 2004) and phosphate (Conkright et al. 2002) are shown for comparison

profiles at both ocean surface and interior ocean (ISAM+OCMIP+updateK_I and ISAM+DGOM+updateK_I runs). This depth-dependent isopycnal diffusivity is physically justified as it reflects the ocean's tendency to diffuse along isopycnal surfaces more rapidly at the ocean surface than at depth (Harvey 1995; England and Rahmstorf 1999).

The modification made in the isopycnal diffusivity greatly improves the simulated phosphate distribution (Figs. 1 and 2) by removing excess phosphate concentrations in the upper low latitude region through more efficient isopycnal mixing between low and mid-to-high latitude oceans. The improvement in the simulation of phosphate is most pronounced by comparing upper ocean phosphate concentrations between 30°S and 30°N between the ISAM+DGOM and ISAM+DGOM+updateK_I runs (Fig. 2). Meanwhile, the model essentially keeps its ability to realistically simulate natural $\Delta^{14}C$ (Figs. 1 and 2, also see Fig. 3 as discussed later). However, neither the model with uniform isopycnal diffusivity (ISAM+OCMIP) or the one with depth-dependent diffusivity (ISAM+OCMIP+updateK_I) is able to simulate well observed inventories of transient tracers. The ISAM+OCMIP+updateK_I run slightly improves the simulation of bomb ^{14}C and anthropogenic CO_2 in the Atlantic, Indian, and Southern Oceans, but worsens their simulations in the Pacific Ocean. The model-observation discrepancy in the Pacific Ocean stems from the overestimation of anthropogenic carbon in the North Pacific, which reflects the difficulty in representing intermediate water formation and tidal process in that region by coarse resolution ocean models (Gnanadesikan et al. 2002; Sarmiento et al. 2004).

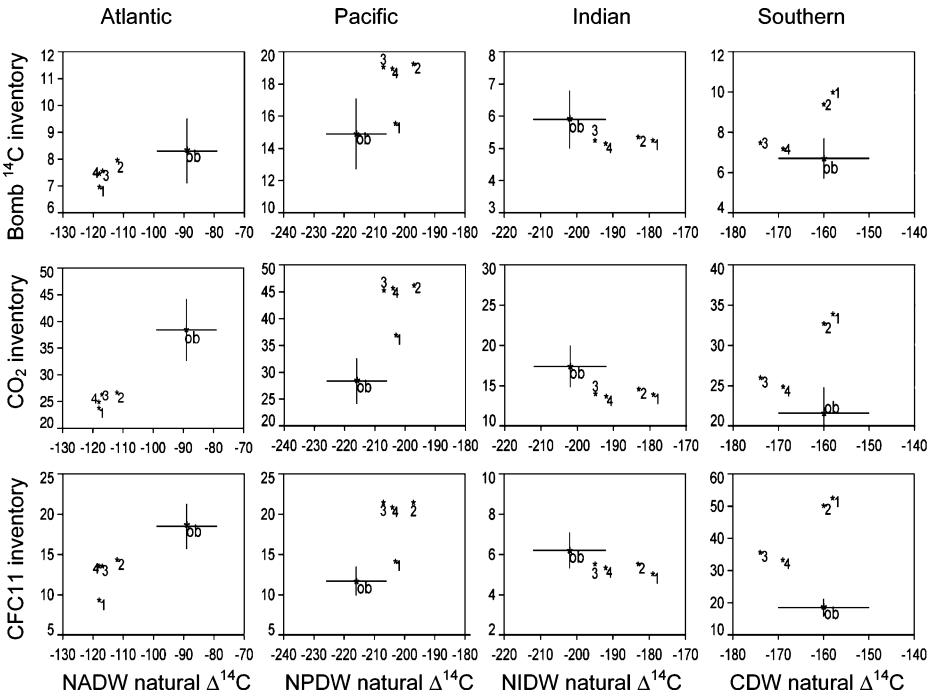

Fig. 3 Observed and modeled inventories of bomb ^{14}C (10^{27} atoms), anthropogenic CO_2 (PgC), and CFC11 (10^7mole) in different ocean basins versus averaged natural Δ^{14}C (per mil) for typical water masses of the corresponding basin from different model runs (1, ISAM+OCMIP; 2, ISAM+OCMIP+updateK_I; 3, ISAM+OCMIP+updateK_I+updateKgas; 4, ISAM+OCMIP+updateK_I+updateKgas+UpdateK_{GM}) Water masses are defined as follows: NADW, North Atlantic Deep Water (0–60°N, 1000–3500 m); NPDW, North Pacific Deep Water (North of Equator, 1500–5000 m); NIDW, North Indian Deep Water (North of Equator, 1500–5000 m); CDW, Circumpolar Deep Water (45–90°S, 1500–5000 m). Error bars of the observation represent 2σ for natural Δ^{14}C and 15% uncertainty for inventories

3.2 Use updated inventory data of bomb ^{14}C

As discussed above, after the modification made in isopycnal diffusivity of the ISAM-2.5D model as suggested by the simulation of phosphate sizeable model-observation discrepancies remain in terms of inventories for bomb ^{14}C and anthropogenic CO_2 (Table 3). Here we examine whether updated observational estimates of bomb ^{14}C inventory can provide new insight about parameterization of air–sea exchange, and thus help to reduce the model-data discrepancy. For a more complete comparison between model and observed inventories of transient tracers, we include the simulation of another transient tracer, CFC11, based on the OCMIP protocol.

The flux of transient tracers from the atmosphere to ocean depends on the partial pressure difference of a certain gas between the atmosphere and ocean surface and the rate of air–sea exchange with the latter usually being parameterized as a function of wind speed and temperature. The most widely used parameterization of air–sea gas exchange assumes a quadratic dependence of air–sea exchange on wind speed (Wanninkhof 1992): $\mathrm{Kgas} = \mathrm{f}\,\mathrm{u}^2(\mathrm{Sc}/660)^{-1/2}$ (Kgas is the rate of air–sea gas exchange, u is the wind speed, Sc is the Schmidt number as a function of temperature, and f is a scaling factor). The scaling factor f is traditionally calibrated to obtain a global mean air–sea exchange rate of Broecker et al. (1995) based on the bomb ^{14}C data measured during the mid-1970s survey of Geochemical

Table 3 Simulated and observational-based inventories of bomb ^{14}C, anthropogenic CO_2, and CFC11 in the mid-1990s in various ocean basins

	Model runs[a]				Observational estimate
	I	II	III	IV	Key et al. (2004)[b]
	Bomb ^{14}C (10^{27} atoms)[c]				
Atlantic	7.1	8.1	7.7	7.6	8.3 (7.1–9.5)
Pacific	15.6	19.3	19.1	19.0	14.9(12.7–17.1)
Indian	5.4	5.5	5.4	5.3	5.9(5.0–6.8)
Southern	9.9	9.3	7.4	7.1	6.7 (5.7–7.7)
Global	38.0	42.2	39.6	39.0	35.8(30.5–41.1)
	CO_2 (PgC=10^{15}gram carbon)				
Atlantic	24.4	27.3	26.9	25.5	38.4(32.6–44.2)
Pacific	37.6	46.9	46.0	46.4	28.4(24.1–32.6)
Indian	14.2	14.9	14.3	14.0	17.4(14.8–20.0)
Southern	35.2	34.0	27.3	26.2	21.6(18.4–24.8)
Global	115.4	123.1	114.5	112.1	105.8(89.9–121.7)
	CFC11(10^7mole)				
Atlantic	8.4	13.4	12.6	12.6	18.5(15.7–21.3)
Pacific	13.1	20.4	20.4	19.8	11.7(9.9–13.5)
Indian	4.7	5.2	5.2	5.0	6.2(5.3–7.1)
Southern	50.0	47.7	33.1	30.8	18.5(15.7–21.3)
Global	76.2	86.7	71.3	67.4	54.9(46.7–63.1)

[a] *I* ISAM-OCMIP, *II* ISAM+OCMIP+updateK_I, *III* ISAM+OCMIP+updateK_I+updateKgas, *IV* ISAM +OCMIP+updateK_I+updateKgas+updateK_{GM}

[b] Range values in the bracket are based on the 15% uncertainty assumed by Key et al. (2004).

[c] Vertical integration stops at 1,600 m as the estimate of bomb ^{14}C inventory given by Key et al. (2004).

Since ocean uptake of transient tracers is independent of biological processes, only results from simulations including the OCMIP biogeochemical component are compared here.

Ocean Section Study (GEOSECS). The scaling factor calibrated this way is commonly used in most modeling studies of the ocean carbon cycle (e.g., ocean carbon cycle models participating the OCMIP project), including the study of Cao and Jain (2005) and the ISAM, ISAM+OCMIP, ISAM+DGOM, and ISAM+OCMIP+K_I runs listed in Table 1.

Since the study of Broecker et al. (1995) updated estimates of bomb ^{14}C inventory have emerged. Key et al. (2004) synthesized the data from the measurements of the Ocean Circulation Experiment (WOCE), the Joint Global Ocean Flux Study (JGOFS), and the Ocean Atmosphere Carbon Exchange Study (OACES) made during the 1990s to estimate the inventory of transient tracers including bomb ^{14}C, anthropogenic CO_2, and CFCs (Global Ocean Data Analysis Project, GLODAP). As pointed out by Peacock (2004), one major bias in the Broecker et al. (1995) analysis is the assumption that the bomb ^{14}C inventory in each 10° latitude band can be obtained from the average of a small number of GEOSECS station-based bomb ^{14}C inventories falling within that band. According to Peacock (2004), this bias may lead to an overestimation of the global bomb ^{14}C inventory by about 15%. Compared to the data obtained from GEOSECS survey, the measurement density for the GLODAP is increased by almost an order of magnitude, which is expected to enhance the reliability of estimated inventories of transient tracers. In addition, independent modeling study on the global radiocarbon budget (Naegler and Levin 2006, Sweeney et al. 2007, Müller et al. 2008) suggested that the estimates of bomb ^{14}C inventory

by Peacock (2004) and Key et al. (2004) are more consistent with our current knowledge of the global excess radiocarbon content compared to that of Broecker et al. (1995).

The updated estimates of bomb ^{14}C inventory calls for a revised calibration of the scaling factor used in the calculation of air–sea gas exchange. We exploit the fact that bomb ^{14}C inventory is equal to the spatially and temporally integrated flux of bomb ^{14}C into the ocean and thus the scaling factor f can be calculated from the observed bomb ^{14}C inventory and evolution of surface CO_2 and ^{14}C following the method of Naegler et al. (2006) (refer to Appendix C for a detailed discussion about the calculation of the scaling factor). We use the ocean basin mean bomb ^{14}C inventory data of Key et al. (2004) to derive the scaling factor for each ocean basin. Compared to the scaling factor calibrated based on the Broecker et al. (1995) analysis, the greatest change is observed in the Southern Ocean, where the updated value is about 55% lower than the previous estimate (Table 2), implying a significant lower air–sea exchange rate in the Southern Ocean.

The updated scaling factor and the resulting rate of air–sea exchange greatly improve the simulated uptake of transient tracers in the Southern Ocean (compare ISAM+OCMIP+updateK_I and ISAM+OCMIP+updateK_I+updateKgas runs in Table 3). With the original scaling factor the model overestimates the ocean inventories of bomb ^{14}C, anthropogenic CO_2, and CFC11 in the Southern Ocean by about 40%, 57%, and 150% respectively, while with the updated scaling factor the model-data discrepancy is reduced to 10%, 25%, and 80% for bomb ^{14}C, anthropogenic CO_2, and CFC11 respectively. Changes in model estimated inventories in other oceans are small as a result of small changes in the rate of air–sea gas exchange.

3.3 Simulate CFC11

After recalibrating the rate of air–sea exchange modeled inventories of bomb ^{14}C and anthropogenic CO_2 in the Southern Ocean are reasonably consistent with the data-based estimates (Table 3 ISAM+OCMIP+updateK_I+updateKgas run). However, the simulated CFC11 inventory in the Southern Ocean is about 80% larger than the observational estimate. Although uncertainties in the representation of air–sea exchange (e.g., wind speed dependence and/or the wind speed data itself) might be partly responsible for this overestimation, the higher-than-observed CFC11 inventory can be partly attributed to an excessive upwelling in the Antarctic Circumpolar Current (ACC) region around 45°S to 65°S. Overly strong ACC upwelling brings excessive deep water free of CFC11 to surface ocean, which, as a result of fast air–sea exchange of CFC11 (an air–sea equilibrium time scale of about 2 weeks), have sufficient time to absorb atmospheric CFC11 before it can be transported away to low latitude oceans, and thus leads to intensive uptake of CFC11 from the atmosphere into the ocean. In contrast, bomb ^{14}C and anthropogenic CO_2 have a much longer time scale of air–sea exchange (about 10 years for bomb ^{14}C and 1 year for anthropogenic CO_2), and therefore water upwelled from the deep ocean is not able to adequately accumulate bomb ^{14}C and anthropogenic CO_2 from the atmosphere before it is transported equatorward. As a result, the excessive ACC upwelling affects CFC11 uptake more than it affects bomb ^{14}C and anthropogenic CO_2. Therefore, the simulation of CFC11 indicates the problem of excessive ACC upwelling more clearly than the simulations of bomb ^{14}C and anthropogenic CO_2.

We now seek ways to further improve the model estimated inventory of transient tracers in the Southern Ocean, especially CFC11, by modifying parameterizations of ocean circulation. As suggested by Gnanadesikan (1999), the rate of Southern Ocean upwelling is determined by the eddy-induced transport and wind-driven Ekman transport (water flow near the ocean surface driven by wind above), with the Ekman transport partially

compensated by the eddy-driven flow. As discussed earlier, in the model parameterization of mesoscale eddies a key parameter is the GM parameter (K_{GM}) that determines the strength of eddy-induced transport. A constant value of 1000 m^2 s^{-1} for the GM parameter has been widely used in previous studies (e.g., Duffy et al. 1997; Hirst and McDougall 1998; Saenko and Weaver 2003) and all our model runs discussed previously. However, as suggested by a number of studies (e.g., Visbeck et al. 1997; England and Rahmstorf 1999; Knutti et al. 2000; Marshall and Radko 2003), the GM parameter is not uniform in the global ocean and possibly related to the vertical and horizontal stratification. To test the effect of a spatially and temporally varying GM parameter on the ocean circulation and tracer uptake, we relate the GM parameter to the isopycnal slope following Visbeck et al. (1997) and Marshall and Radko (2003). (ISAM+OCMIP+updateK_I+updateKgas+updateK_{GM} run) The calculated GM parameter varies between 800 and 2000 m^2 s^{-1} in the modeled Southern Ocean. The overall increase in the GM parameter strengthens the eddy-driven circulation in the Southern Ocean, reducing the ACC upwelling and the effective vertical diffusion. As a result, the simulated inventories of CFC11, bomb ^{14}C, and anthropogenic CO_2 in the Southern Ocean are further reduced by about 5% (compare ISAM+OCMIP+updateK_I+updateKgas and ISAM+OCMIP+updateK_I+updateKgas+updateK_{GM} runs in Table 3). Changes in the GM parameter have a smaller effect on tracer uptake in other ocean basins as a result of diminished role of mesoscale eddies in ocean circulation and tracer transport outside the Southern Ocean (Cao and Jain 2005).

3.4 Synthesis of model comparison

As discussed so far through the simulation of multiple tracers that hold different information about ocean mixing, circulation, and air–sea gas exchange and the inclusion of updated observational data, the ISAM-2.5D model initially constrained by the simulation of $\Delta^{14}C$ has undergone a number of modifications including changes in isopycnal diffusivity, the rate of air–sea gas exchange, and the parameterization of eddy-induced circulation. The performance of different model runs are synthesized in Fig. 3, which compares simulated inventories of transient tracers (e.g., CFC11, bomb ^{14}C, and anthropogenic CO_2) and natural $\Delta^{14}C$ in each ocean basin with corresponding observations. This synthesis comparison of model performance allows one to examine readily how each modification made in model parameterizations affects the model's ability to simulate ocean circulation and the rate of air–sea exchange over decadal to centennial (characterized by simulated inventories of transient tracers) and millennium (characterized by simulated natural $\Delta^{14}C$) time scales at the same time. In general, relative to the original model setup (ISAM+OCMIP run), the step-by-step modifications made in the parameterization of ocean mixing and air–sea gas exchange improve the simulation of tracers in the Southern, Indian, and Atlantic Ocean, but somewhat worsens simulated transient tracer inventories in the Pacific Ocean. Modifications made in the model greatly improve the model performance in simulating inventories of bomb ^{14}C, anthropogenic CO_2, and CFC11 in the Southern Ocean while the simulated $\Delta^{14}C$ in that region remains within the uncertainly range of data-based estimates. Another pronounced improvement is observed in the Indian Ocean where modified models are characterized by older North Indian Deep Water (NIDW) (more negative natural $\Delta^{14}C$) that is in closer agreement with the observation. In the Atlantic Ocean the updated model slightly improves the simulated uptake of transient tracers, while maintaining the skill of simulating $\Delta^{14}C$. In the Pacific Ocean, however, modified models lead to larger model-observation discrepancy in the uptake of transient tracers. As discussed earlier, this discrepancy mainly stems from the

North Pacific where coarse resolution models such as the ISAM-2.5D have difficulty in capturing ocean dynamics in that region. When the tracer distribution for each model run is compared at the global scale, improvement is observed for all physical metrics, especially for salinity and bomb ^{14}C (Appendix D).

The step-by-step modification made in the model does not necessarily lead to uniform movement toward observations. For example, updated GM parameter leads to slightly worse simulation of natural $\Delta^{14}C$ in the Indian Ocean. In the Atlantic Ocean, both updated air–sea gas exchange rate and GM parameter lead model results to be further away from observations.

3.5 Implication for oceanic uptake of anthropogenic CO_2

We further investigate the impact of the previously discussed modifications in the model setup on the simulated oceanic uptake of anthropogenic CO_2. The model is forced with observed atmospheric CO_2 concentrations between year 1800 and 1999 (Keeling and Whorf 2000) and with the atmospheric CO_2 concentrations projected by Kheshgi and Jain (2003) based on IPCC IS92a emission scenario for the period 2000 to 2100.

At the global scale, simulated historical uptake of anthropogenic CO_2 for all model runs is within the uncertainty range of observational-based estimates (Table 4). This indicates that current observational-based estimates of global ocean CO_2 uptake are not sufficient to constrain the parameters that govern the model's representation of ocean physics and air–

Table 4 Model simulated cumulative oceanic uptake of anthropogenic CO_2 in PgC (1 PgC=10^{15} gram carbon) for runs listed in Table 1

	1800–1994		1990–1999		1800–2100	
	Global	Southern	Global	Southern	Global	Southern
This study						
ISAM+OCMIP	115	34	20.0	6.6	540	190
ISAM+OCMP+updateK_I	128	33	22.2	6.7	584	192
ISAM+OCMIP+ +updateK_I+updateKgas	119	27	20.6	4.9	537	137
ISAM+OCMIP+ +updateK_I+updateKgas+ updateK_{GM}	118	24	20.9	4.8	531	133
Other studies						
McNeil et al. (2003)[a]			20.0± 4			
Sabine et al. (2004) [b]	118± 19					
Mikaloff Fletcher et al. (2006)[c]			22.0± 2.5			
Manning and Keeling (2006)[d]			19±6			

The model is forced by observed atmospheric CO_2 concentrations between year 1800 and 1999 (Keeling and Whorf 2000) and by the atmospheric CO_2 concentrations projected by Kheshgi and Jain (2003) based on IPCC IS92a emission scenario for the period 2000 to 2100. Observational-based estimates for the global CO_2 uptake using different methods are listed here for comparison.

[a] Based on CFC observations combined with the atmospheric CO_2 history

[b] Based on inorganic carbon measurement during the 1990s and a tracer-based separation method

[c] Based on a combination of data-based estimates of anthropogenic CO_2 in the ocean and model inversions

[d] Based on the measurement of atmospheric O_2/N_2 ratio and atmospheric CO_2 concentrations

sea gas exchange. After a series of model modifications the simulated CO_2 uptake by the global ocean is quite similar to that of the initial run. Each modification in the model structure leads to a noticeable change in CO_2 uptake by the ocean, but their effects compensate each other. Increased isopycnal diffusivity increases CO_2 uptake outside the Southern Ocean, while reduced air–sea gas exchange rate and modified parameterization of eddy-induced circulation decreases CO_2 uptake in the Southern Ocean. In our model, these effects approximately offset each other. By years 2000 and 2100, increased isopycnal diffusivity alone increases the cumulative uptake of CO_2 by 15 and 44 PgC respectively, while reduced air–sea gas exchange rate and modified parameterization of eddy-induced circulation decreases CO_2 uptake by 12 and 53 PgC respectively. As a result, the difference in the cumulative global ocean CO_2 uptake by year 2100 between the initial run (540 PgC for the ISAM+OCMIP run) and updated run (531 PgC for the ISAM+OCMIP+ updateK_I+ updateKgas+updateK_{GM} run) is only 2%, but the difference in the simulated Southern Ocean CO_2 uptake is more substantial (Fig. 4, Table 4) (30% difference between 190 PgC of the ISAM+OCMIP run and 133 PgC of ISAM+OCMIP+updateK_I+updateKgas+updateK_{GM} run). The considerably diminished role of the Southern Ocean in the global CO_2 uptake in the updated model can be considered as a more realistic projection of carbon uptake by the Southern Ocean, given the fact that the updated model yields a more realistic simulation of transient tracer inventories in that region.

4 Discussion and conclusions

In this study we have demonstrated how new information can be acquired about the parameterization of ocean circulation and air–sea gas exchange in ocean carbon cycle models through the simulation of multiple tracers and the use of updated observational data.

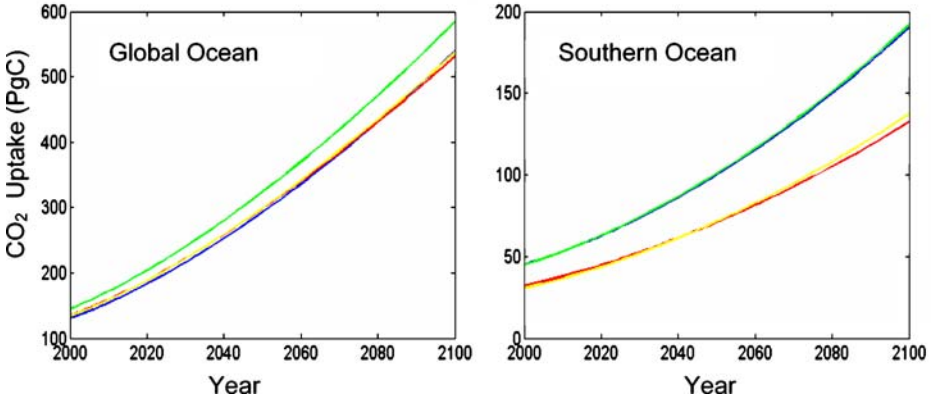

Fig. 4 Model-simulated cumulative ocean uptake of anthropogenic CO_2 for the global and Southern Ocean based on four model runs as listed in Table 1 (blue: ISAM+OCMIP; green: ISAM+OCMIP+updateK_I; yellow: ISAM+OCMIP+updateK_I+updateKgas; red: ISAM+OCMIP+updateK_I+updateKgas+updateK_{GM}. Between year 1800 and 1999 simulations are forced by observed CO_2 concentrations (Keeling and Whorf 2000) and between year 2000 and 2100 simulations are forced by the atmospheric CO_2 concentrations projected by Kheshgi and Jain (2003) based on IPCC IS92a emission scenario

This new information leads to changes in model parameters and the global and regional pattern of simulated carbon uptake.

Through the simulation of $\Delta^{14}C$ in the ISAM-2.5D model we have identified the importance of representing subgrid scale ocean mixing in terms of isopycnal diffusion with the inclusion of a parameterization of eddy-induced circulation. However, the strength of both isopycnal diffusion and eddy-induced circulation is poorly constrained by the simulation of $\Delta^{14}C$. The modeling of additional tracers helps us to better constrain these parameterizations. The simulation of biogeochemical tracers like phosphate reveals the weak isopycnal diffusion in the modeled upper ocean that is not clearly visible in the simulation of $\Delta^{14}C$, while the modeling of CFC11 demonstrates the importance of linking the GM parameter used in the parameterization of eddy-induced circulation to density structure of the ocean. In addition, the updated observational data of bomb ^{14}C inventory enables us to recalibrate the rate of air–sea gas exchange.

After these progressive modifications made in the model structure, the model greatly improves its performance in simulating uptake of transient tracers in the Southern Ocean and natural $\Delta^{14}C$ in the Indian Ocean, while essentially maintaining its ability in simulating other aspects of tracer distribution in different oceans. A pronounced exception is in the Pacific Ocean where the increased isopycnal diffusivity leads to larger model-observation discrepancy in the uptake of transient tracers. A better representation of the intermediate water formation in the North Pacific by including processes such as tidal mixing seems to be needed to improve the simulation of ocean circulation in that region (Gnanadesikan et al. 2002; Sarmiento et al. 2004). Nevertheless, our modeling practice clearly demonstrates the value of simulating multiple tracers and using updated observations in providing complementary information about the parameterization of ocean circulation and air–sea gas exchange. A comprehensive estimation of model parameterizations in a more stringent procedure may require optimizing a whole set of model parameters simultaneously and objectively with ensemble model runs (e.g., Edwards and Marsh 2005).

The simulation of additional tracers provide additional information about the parameterization of ocean physics and air–sea gas exchange, but does not necessarily suggest a unique solution to identified problems. We improve the phosphate simulation by modifying isopycnal diffusivity. Alternatively, the excessive phosphate concentrations might also be caused by excessive deep upwelling in the equatorial ocean, which was found can be partly fixed by increasing either the horizontal (Aumont et al. 1999) or vertical resolution (Müller et al. 2006). The sensitivity of the ISAM-2.5D modeled ocean dynamics to the model resolution is an open question and merits further investigation. Similarly, the excessive upwelling in the Southern Ocean could also be reduced by forcing the model with weaker wind. Improvement in both observational and theoretical studies are needed to determine a unique solution to problems indicated by model simulations.

Changes in the parameterization of both ocean mixing and air–sea gas exchange have sizeable effects on estimated carbon uptake. In our modeling practice here, change in isopyncal diffusivity increases the estimated CO_2 uptake outside the Southern Ocean, while the subsequent change to the air–sea gas exchange rate decreases uptake in the Southern Ocean, leading to a small change in the carbon uptake at the global scale. There is a parallel here to the concept of negative learning (Oppenheimer et al., this issue), in which new information can move a model outcome further from the right answer. In this case, observation data of global ocean CO_2 uptake do not provide a sufficient constraint to test the performance of different model runs, but because successive steps move the estimated uptake in opposite directions, one of the steps represents negative learning. Because the

ocean carbon cycle is a complex system, and improvement in one aspect of it (e.g., isopycnal mixing) will not necessarily improve the estimate of an integrative model outcome such as cumulative uptake.

In contrast, the change in estimates of the regional distribution of CO_2 uptake across models moves in one direction and is substantial. The considerably diminished role of the Southern Ocean in the global CO_2 uptake in the updated model reflects a more realistic projection of carbon uptake by the Southern Ocean given the fact that the updated model yields a more realistic simulation of transient inventories in that region. This point is of particular importance since the magnitude of the CO_2 sink in the Southern Ocean is heavily disputed (e.g, Roy et al. 2003; Mikaloff Fletcher et al. 2006).

Although this study is conducted using a zonally averaged ocean model in the framework of an earth system model of intermediate complexity, the insight gained here can be applied to more comprehensive 3-D models used to project climate change. The simulation of multiple physical, chemical, and biological tracers, together with the aid of available and upcoming observational data of ocean physics and biology, is expected to reveal more aspects of the parameterization of ocean mixing and air–sea gas exchange in 3-D ocean carbon cycle models with higher spatial resolutions and more sophisticated ocean dynamics. For example, a number of studies have suggested that the simulation of biogeochemical tracers can provide additional opportunity to evaluate 3-D ocean physical models, in addition to physical metrics (Matsumoto et al. 2004; Doney et al. 2004; Müller et al. 2006; Najjar et al. 2007). With increased measurement density and data availability, there is also a growing interest in using the simulation of noble gases such as argon to constrain modeled ocean mixing and air–sea gas exchange (e.g., Gehrie et al. 2006; Müller et al. 2006; Ito et al. 2007). Insight gained about the model representations of ocean mixing and air–sea exchange through model simulations and observations of multiple tracers can help to improve model's ability to simulate CO_2 uptake by the ocean, and ultimately lead to a more reliable projection of atmospheric CO_2.

Appendix A: Conversion from ^{14}C to $\Delta^{14}C$

To facilitate model-data comparison, a frequently used notation in the simulation of radiocarbon is $\Delta^{14}C$, which is defined as (Stuiver and Pollach 1977):

$$\Delta^{14}C = \left[\delta^{14}C - 2\left(\delta^{13}C + 0.025\right)\left(1 + \delta^{14}C/1000\right)\right] \tag{A1}$$

$$\delta^{14}C = \left(\frac{^{14}C/^{12}C}{(^{14}C/^{12}C)_{std}} - 1\right) * 1000 \tag{A2}$$

where $(^{14}C/C)_{std} = 1.176 \times 10^{-12}$ is the oxalic acid standard. As an approximation, we assume $\delta^{13}C = 0‰$ in the above calculation.

Appendix B: Description of the ISAM-2.5D ocean biogeochemical cycle component

In this study we have incorporated two different models of ocean biogeochemical cycle in the ISAM-2.5D. The first one is the ocean biogeochemistry model based on OCMIP protocol (http://www.ipsl.jussieu.fr/OCMIP), referred to as OCMIP model, and the second

one is the marine ecosystem model based on Le Quéré et al. (2005), referred to as Dynamic Green Ocean Model (DGOM).

The OCMIP model is an ocean biogeochemistry model that parameterizes the process of marine biology in terms of geochemical fluxes without the explicit representation of marine ecosystems and food web processes. It includes five prognostic variables: inorganic phosphate, semi-labile dissolved organic phosphorus (DOP), dissolved oxygen (O_2), dissolved inorganic carbon (DIC), and alkalinity. Following the OCMIP protocol, production of organic matter is simulated by restoring modeled phosphate towards an observation-based climatology (Conkright et al. 2002) in the euphotic zone (upper 100 m ocean in the model) with a time scale of 30 days. Two thirds of the organic production goes to DOP with a remineralization lifetime of 6 months, and the remainder goes to particulate organic matter (POM), which is remineralized instantly in the water column below the euphotic zone following a power law function with depth. The complete model description and related parameters are given in the OCMIP protocol (http://www.ipsl.jussieu.fr/OCMIP).

The DGOM model explicitly represents marine ecosystem community, the functioning of plankton, and a suite of food web processes. It includes three types of nutrients (phosphate, silicic acid, and iron), three phytoplankton functional types (PFTs) (nanophytoplankton, diatoms, and coccolithophorids), two size classes of zooplankton (microzooplankton, mesozooplankton), two size classes of particulate organic matter (big and small POM), and dissolved organic matter (DOM). In addition to ecosystem variables, the model simulates DIC, total alkalinity, and dissolved oxygen. Key biological processes represented by the module include biological production, multiple nutrient limitation of phytoplankton growth, food web processes between different groups of phytoplankton and zooplankton, aggregation/disaggregation and sinking of particulate material, and remineralization of organic matter.

Appendix C: Calibration of scaling factor

The scaling factor f used in the calculation of air–sea gas exchange ($K_{\mathrm{gas}} = f\, u^2(\mathrm{Sc}/660)^{-1/2}$ K_{gas} is the rate of air–sea gas exchange, u is the wind speed, Sc is the Schmidt number as a function of temperature, and f is a scaling factor) is calculated from the observed bomb ^{14}C inventory and simulated oceanic carbon uptake following Naegler et al. (2006):

$$f = \frac{I(t)}{\int_{t0}^{t}\int_{S} u^2 (Sc/660)^{-1/2}\alpha\left(R_A pCO_2^A - R_o pCO_2^O\right)\mathrm{d}S\mathrm{d}t} \tag{C1}$$

In the above equation, $I(t)$ is the data-based bomb ^{14}C inventory at time t and t_0 represents pre-bomb time (year 1954). S is the ocean area and α is the solubility of CO_2. u is the wind speed and Sc is the Schmidt number. pCO_2^A and pCO_2^O are CO_2 partial pressure in the atmosphere and ocean surface. R_A and R_o are $^{14}C/^{12}C$ ratio in the atmosphere and the surface ocean. In our calculation, pCO_2^A and R_A are taken from the observation (Enting et al. 1994; Keeling and Whorf 2000). pCO_2^O and R_o are from model simulations. Schmidt number Sc and CO_2 solubility α are calculated from observed temperature and salinity. We applied the above equation at both the global and ocean basin scale using the bomb ^{14}C inventory data of Peacock (2004) and Key et al. (2004) and derived the scaling factor for the global ocean as well as each basin. Since the Peacock (2004) data are for the mid-1970s and the Key et al. (2004) data are for the mid-1990s, t is taken to be year 1975 when using the Peacock (2004) data and year 1995 when using the data of Key et al. (2004).

The quality of calculated f based on the above equation is affected by the uncertainty in model-simulated CO_2 partial pressure at the ocean surface pCO_2^O and the surface ocean

$^{14}C/^{12}C$ ratio R_o. To correct potential bias in calculated f and have a direct comparison with previous studies in which the scaling factor is calibrated against the global mean air–sea exchange rate estimated by Broecker et al. (1995), we take the following procedures. First, we directly adjusted f to obtain a global mean air–sea exchange rate of 21.9 cm/hr inferred from Broecker et al. (1995). This yields a value of 0.50 for f. Then we use Eq. (C1) to calculate f using the global inventory data of Broecker et al. (1985, 1995). In this way, we obtain a value of 0.37 for f. The difference of f between these two calculations can be attributed to the different methods used in estimating the evolution of ocean surface ^{14}C: Broecker et al. (1995) used observed surface ^{14}C history at a single station to represent the global profile, while we estimate ^{14}C from model simulations. To correct this difference, we calculated a correction factor fac=0.37/0.50 and applied it to the calculated f based on Eq. (C1) in all cases.

Appendix D

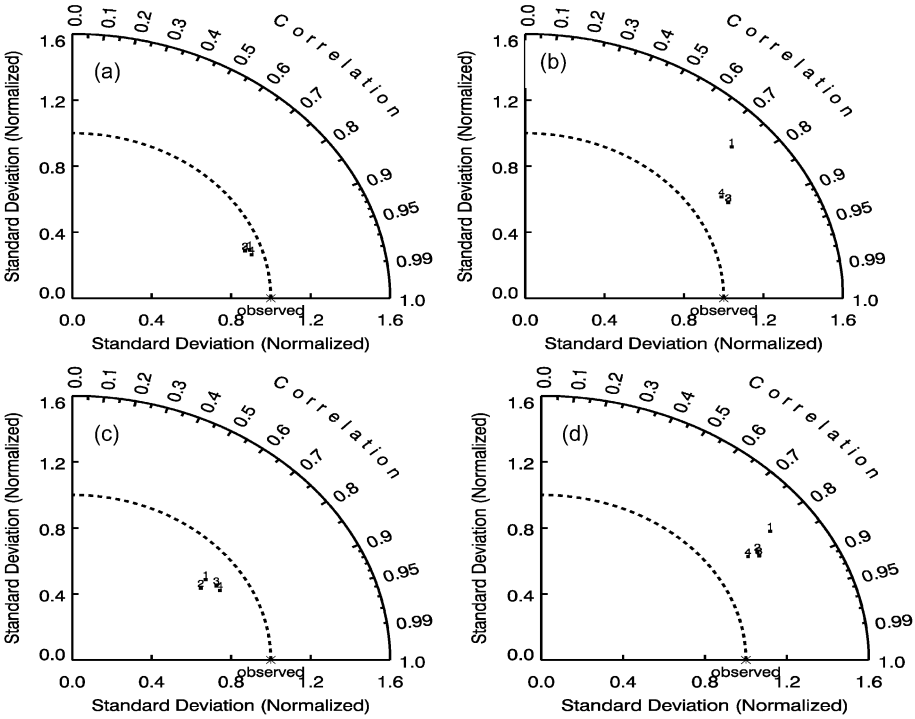

Fig. 5 Comparison of model-simulated (**a**) temperature, (**b**) salinity, (**c**) natural $\Delta^{14}C$, and (**d**) bomb ^{14}C in the global ocean with corresponding observations using the Taylor diagram (Taylor 2001) for different model runs (1, ISAM+OCMIP; 2, ISAM+OCMIP+updateK_I; 3, ISAM+OCMIP+updateK_I+updateKgas; 4, ISAM +OCMIP+updateK_I+updateKgas+updateK_{GM}).). In some cases, the simulated spatial patterns of these physical metrics are similar to each other. Therefore, the corresponding symbols overlap. The diagram is read as follows: For each point the radial distance from the origin to the point gives the pattern standard deviations, and the azimuthal positions give the correlation with observations. The distance between the observation and model represents the centered RMS error. Each statistic variable is normalized by the standard deviation of the corresponding observation

References

Anderson LA, Sarmiento JL (1995) Global ocean phosphate and oxygen simulations. Glob Biogeochem Cycles 9(4):621–636

Aumont O, Orr J, Monfray P, Madec G, Maier-Reimer E (1999) Nutrient trapping in the equatorial Pacific: the ocean circulation solution. Glob Biogeochem Cycles 13:351–369

Broecker WS, Peng T-H, Ostlund G, Stuiber M (1985) The distribution of bomb radiocarbon in the ocean. J Geophys Res 90:6953–6970

Broecker WS, Sutherland S, Smethie W, Peng T-H, Ostlund G (1995) Oceanic radiocarbon: separation of the natural and bomb components. Glob Biogeochem Cycles 9:263–288

Cao L, Jain A (2005) An Earth system model of intermediate complexity: simulation of the role of ocean mixing parameterizations and climate change in estimated uptake for natural and bomb radiocarbon and anthropogenic CO_2. J Geophys Res 110:C09002 DOI 10.1029/2005JC002919

Conkright ME, Garcia HE, O'Brien TD, Locarnini RA, Boyer TP, Stephens C, Antonov JI (2002) World Ocean Atlas 2001, vol. 4, Nutrients, NOAA Atlas NESDIS 52. Natl Oceanic and Atmos Admin, Silver Spring, MD

Doney SC et al (2004) Evaluating global ocean carbon models: the importance of realistic physics. Glob Biogeochem Cycles 18:GB3017 DOI 10.1029/2003GB002150

Duffy PB, Caldeira K, Selvaggi J, Hoffert MI (1997) Effects of subgrid-scale mixing parameterizations on simulated distributions of natural ^{14}C, temperature, and salinity in a three-dimensional ocean general circulation model. J Phys Oceanogr 27:498–253

Dutay J-C et al (2002) Evaluation of ocean model ventilation with CFC-11: comparison of 13 global ocean models. Ocean Model 4:89–120

Edwards NR, Marsh R (2005) Uncertainties due to transport-parameter sensitivity in an efficient 3-D ocean-climate model. Clim Dyn 24:415–433

England MH, Rahmstorf S (1999) Sensitivity of ventilation rates and radiocarbon uptake to subgrid-scale mixing in ocean models. J Phys Oceanogr 29:2802–2827

England MH, Maier-Reimer E (2001) Using chemical tracers to assess ocean models. Rev Geophys 39:29–70

Enting IG, Wigley TML, Heimann M (1994) Future emissions and concentrations of carbon dioxide: Key ocean/atmosphere/land analyses, Tech. Rep. 31, Div. of Atmos. Res., Commonw. Sci. and Ind. Res. Organ., Melbourne

Fiadeiro ME (1982) Three-dimensional modeling of tracers in the deep Pacific Ocean, 2, Radiocarbon and the circulation. J Mar Res 40:537–550

Gehrie E, Archer D, Emerson S, Stump C, Henning C (2006) Subsurface ocean argon disequilibrium reveals the equatorial Pacific shadow zone. Geophys Res Lett 33:L18608 DOI 10.1029/2006GL026935

Gent PR, Willebrand J, McDougall TJ, McWilliams JC (1995) Parameterizing eddy-induced tracer transports in ocean circulation models. J Phys Oceanogr 25:463–474

Gnanadesikan A (1999) A simple predictive model for the structure of the oceanic pycnocline. Science 283:2077–2079

Gnanadesikan A, Slater RD, Gruber N, Sarmiento JL (2002) Oceanic vertical exchange and new production: a comparison between models and observations. Deep Sea Res, Part II 49:363–401

Guilderson T, Caldeira K, Duffy PB (2000) Radiocarbon as a diagnostic tracer in ocean and carbon cycle modeling. Glob Biogeochem Cycles 14:887–902

Harvey LDD (1995) Impact of isopycnal diffusion in a two-dimensional ocean model. J Phys Oceanogr 25:2166–2176

Harvey LDD (2001) A quasi-one-dimensional coupled climate-carbon cycle model: Part II. The carbon cycle component. J Geophys Res 106:22355–22372

Hirst AC, McDougall TJ (1998) Meridional overturning and dianeutral transport in a *z*-coordinate ocean model including eddy-induced advection. J Phys Oceanogr 28:1205–1223

Ito T, Deutsch C, Emerson S, Hamme RC (2007) Impact of diapycnal mixing on the saturation state of argon in the subtropical North Pacific. Geophys Res Lett 34:L09602 DOI 10.1029/2006GL029209

Jain AK, Kheshgi HS, Hoffert MI, Wuebbles DJ (1995) Distribution of radiocarbon as a test of global carbon-cycle models. Glob Biogeochem Cycles 9:153–166

Joos F, Plattner G-K, Stocker TF, Marchal O, Schmittner A (1999) Global warming and marine carbon cycle feedbacks on future atmospheric CO_2. Science 284:464–467

Keeling CD, Whorf TP (2000) Atmospheric CO_2 records from sites in the SIO air sampling network. Trends: a compendium of data on global change. Carbon Dioxide Information Analysis Center, Oak Ridge National Laboratory, Oak Ridge, TN., USA

Key RM, Kozyr A, Sabine CL, Lee K, Wanninkhof R, Bullister JL, Feely RA, Millero FJ, Mordy C, Peng T-H (2004) A global ocean carbon climatology: results from Global Data Analysis Project (GLODAP). Glob Biogeochem Cycles 18:GB4031 DOI 10.1029/2004GB002247

Kheshgi HS, Jain AK (2003) Projecting future climate change: implications of carbon cycle model intercomparision. Glob Biogeochem Cycles 17(2):1047 DOI 10.1029/2001GB001842
Knutti R, Stocker TF, Wright DG (2000) The effects of sub-grid-scale parameterizations in a zonally averaged ocean model. J Phys Oceanogr 30:2738–2752
Le Quéré C et al (2005) Ecosystem dynamics based on plankton functional types for global ocean biogeochemistry models. Glob Chang Biol 11:1–25 DOI 10.1111/j.1356-2486.2005.0010004.x
Maier-Reimer E (1993) Geochemical cycles in an ocean general circulation model: preindustrial tracer distributions. Glob Biogeochem Cycles 7:645–677
Manning AC, Keeling RF (2006) Global oceanic and land biotic carbon sinks from the Scripps atmospheric oxygen flask sampling network. Tellus 58:95–116
Marchal O, Stocker TF, Joos F (1998) A latitude-depth, circulation-biogeochemical ocean model for paleoclimate studies: model development and sensitivities. Tellus 50B:290–316
Marshall JC, Radko T (2003) Residual mean solutions for the Antarctic Circumpolar Current and its associated overturning circulation. J Phys Oceanogr 33:2341–2354
Matsumoto K et al (2004) Evaluation of ocean carbon cycle models with data-based metrics. Geophys Res Lett 31:L07303 DOI 10.1029/2003GL018970
McNeil BI, Matear RJ, Key RM, Bullister JL, Sarmiento JL (2003) Anthropogenic CO_2 uptake by the ocean based on the global chlorofluorocarbon data set. Science 299:235–239
Melnikov NB, O'Neill BC (2006) Learning about the carbon cycle from global budget data. Geophys Res Lett 33:L02705 DOI 10.1029/2005GL023935
Mikaloff Fletcher SE et al (2006) Inverse estimates of anthropogenic CO_2 uptake, transport, and storage by the ocean. Glob Biogeochem Cycles 20:GB2002 DOI 10.1029/2005GB002530
Müller SA, Joos F, Edwards NR, Stocker TF (2006) Water mass distribution and ventilation time scales in a cost-efficient, three-dimensional ocean model. J Climate 19(21):5479–5499 DOI 10.1175/JCLI3911.1
Müller et al (2008) Gas exchange rates and modeled regional inventories of excess radiocarbon. Glob Biogeochem Cycles. DOI 10.1029/2007GB003065 (in press)
Naegler T, Levin I (2006) Closing the global radiocarbon budget 1945–2005. J Geophys Res 111:D12311 DOI 10.1029/2005JD006758
Naegler T, Ciais P, Rodgers KB, Levin I (2006) Excess radiocarbon constraints on air–sea gas exchange and the uptake of CO2 by the oceans. Geophys Res Lett 33:L11802 DOI 10.1029/ 2005GL025408
Najjar RG, Sarmiento JL, Toggweiler JR (1992) Downward transport and fate of organic matter in the ocean: simulations with a general circulation model. Glob Biogeochem Cycles 6:45–76
Najjar RG et al. (2007) Impact of circulation on export production, dissolved organic matter and dissolved oxygen in the ocean: Results from phase II of the Ocean Carbon-cycle Model Intercomparison Project (OCMIP-2). Global Biogeochem Cy 21:GB3007. DOI 10.1029/2006GB002857
Oeschger H, Siegenthaler U, Schotterer U, Guglemann A (1975) A box-diffusion model to study the carbon dioxide exchange in nature. Tellus 27:168–292
O'Neill BC, Melnikov NB (2007) Learning about parameter and structural uncertainty in carbon cycle models. Climatic Change (in press)
Orr JC et al (2001) Estimates of anthropogenic carbon uptake from four 3-D global ocean models. Glob Biogeochem Cycles 15:43–60
Peacock S (2004) Debate over the ocean bomb radiocarbon sink: closing the gap. Glob Biogeochem Cycles 18:GB2022 DOI 10.1029/2003GB002211
Prentice IC et al (2001) The carbon cycle and atmospheric carbon dioxide. In: Houghton JT et al (ed) Climate change 2001: the scientific basis. Contribution of working group I to the third assessment report of the intergovernmental panel on climate change. . Cambridge University Press, Cambridge, United Kingdom and New York, NY, USA
Redi MH (1982) Oceanic isopycnal mixing by coordinate rotation. J Phys Oceanogr 12:1154–1158
Robitaille DY, Weaver AJ (1995) Validation of sub-grid scale mixing schemes using CFCs in a global ocean model. Geophys Res Lett 22:2917–2920
Roy T, Rayner P, Matear R, Francey R (2003) Southern hemisphere ocean CO_2 uptake: reconciling atmospheric and oceanic estimates. Tellus 55B:701–710
Sabine CL et al (2004) The oceanic sink for anthropogenic CO_2. Science 305:367–370
Saenko OA, Weaver AJ (2003) Southern Ocean upwelling and eddies: Sensitivity of the global overturning to the surface density range. Tellus 55A:106–111
Sarmiento JL, Orr JC, Siegenthaler U (1992) A perturbation simulation of CO_2 uptake in an ocean general circulation model. J Geophys Res 97(C3):3621–3645
Sarmiento JL, Gruber N, Brzezinski MA, Dunne JP (2004) High latitude controls of thermocline nutrients and low latitude biological productivity. Nature 427:56–60
Siegenthaler U, Joos F (1992) Use of a simple model for studying oceanic tracer distributions and the global carbon cycle. Tellus, 44B, 186–207

Stocker TF, Broecker WS, Wright DG (1994) Carbon uptake experiments with a zonally averaged global ocean circulation model. Tellus 46B:103–122

Stuiver M, Pollach HA (1977) Discussion and reporting of ^{14}C data. Radiocarbon 19:355–363

Sweeney C, Gloor E, Jacobson AR, Key RM, McKinley G, Sarmiento JL, Wanninkhof R (2007) Constraining global air-sea gas exchange for CO_2 with recent bomb ^{14}C measurements. Glob Biogeochem Cycles 21:GB2015 DOI 10.1029/2006GB002784

Taylor KE (2001) Summarizing multiple aspects of model performance in single diagram. J Geophys Res 106:7183–7192

Toggweiler JR, Dixon K, Bryan K (1989a) Simulations of radiocarbon in a coarse-resolution world ocean model 1, Steady-state prebomb distributions. J Geophys Res 94:8217–8242

Toggweiler JR, Dixon K, Bryan K (1989b) Simulations of radiocarbon in a coarse-resolution world ocean model 2, Distributions of bomb-produced carbon 14. . Geophys Res 94:8243–8264

Visbeck M, Marshall J, Haine T, Spall M (1997) Specification of eddy transfer coefficients in coarse-resolution ocean circulation models. J Phys Oceanogr 27:381–402

Wanninkhof R (1992) Relationship between wind-speed and gas-exchange over the ocean. J Geophys Res 97:7373–7382